Speed Control of IPMSM Based on Series Connection Leading Correction Linear Active Disturbance Rejection Controller

Yangyang Cui, Zhonggang Yin, *Member, IEEE*, Fengtao Gao, Yanping Zhang, *Member, IEEE*, Yiqi Liu, *Member, IEEE*, and Jing Liu

***Abstract*—In the interior permanent magnet synchronous motor drive system, the conventional linear active disturbance rejection controller (LADRC) has coupling problems with tracking and antidisturbance under different operating conditions and various complex disturbance conditions due to the influence of bandwidth. To solve abovementioned problem, a series connection leading correction LADRC (SCLC-LADRC) is proposed in this article. As the core of SCLC-LADRC, the SCLC linear extended state observer (SCLC-LESO) is composed of the total disturbance transfer function of the conventional linear extended state observer and a series connection leading correction network. As a result, the estimation range of the LESO for total disturbance is expanded, and the problem of system oscillation caused by excessive observer bandwidth is also solved. Finally, the validity and availability of the proposed method are proved through theoretical analysis and experiments.**

***Index Terms*—Interior permanent magnet synchronous motor, linear active disturbance rejection controller, linear extended state observer, series connection leading correction network, speed control.**

I. Introduction

PERMANENT magnet synchronous motor (PMSM) are extensive used in electric vehicles, aerospace, computer numerical control machine tools, and military industries because of its good dynamic performance, structure compact, and high reliability [1], [2]. According to the installation position of the rotor permanent magnet, the PMSM can be separated into interior permanent magnet synchronous motor (IPMSM) and surface-mounted permanent magnet synchronous motor (SPMSM) [3]. Among them, compared to SPMSM, the IPMSM has received widespread attention for its ability to improve load capacity by utilizing its reluctance torque. At present, the IPMSM drive systems are mostly implemented using dual closed-loop vector control method bottomed on maximum torque per ampere control [4]. The speed loop controller is used as the given instruction signal for the current loop controller in the dual closed-loop speed control system, and has a pivotal position in the entire drive system [5].

When the motor drive system is affected by inertia mismatch and load disturbance under different operating conditions, its output speed and torque have good dynamic tracking characteristic and antidisturbance ability [6]. The conventional proportional integral (PI) speed loop controller based on linear negative feedback occupies a dominant position in IPMSM drive systems due to its simple structure, easy parameter tuning, and high reliability [7]. However, when the motor operates under harsh operating conditions such as extremely low-speed and ultrahigh speed, and is affected by inertia mismatch and load disturbance simultaneously, it is difficult for conventional PI controllers to effectively regulate it [8]. Based on the abovementioned analysis, sliding mode control [9], model predictive control [10], internal model control [11], disturbance observer control [12], fuzzy control [13], neural network control [14], active disturbance rejection control (ADRC) [15], and others are widely used in the IPMSM drive systems. The ADRC abandons the concept of "model theory" in the conventional control theory, takes "engineering cybernetics" as the core, and compensates the total disturbance in real time through extended state observer, combined with tracking differentiator (TD), and state error feedback [16]. However, the nonlinear function is adopted by the nonlinear ADRC, which has complex structure and numerous parameters, and is not conducive to engineering applications [17]. To solve the problem of difficult parameter tuning, a linear active disturbance rejection controller (LADRC) is proposed by Prof. Z. Gao [18] from Cleveland University in the United States, which associates ADRC parameters with

Manuscript received 30 May 2023; revised 24 October 2023; accepted 3 December 2023. Date of publication 8 December 2023; date of current version 26 January 2024. This work was supported in part by the National Natural Science Foundation of China under Grants 52177194 and 52207222, in part by Nature Science Basic Research Plan in Shaanxi Province under Grants 2022JQ-538 and 2022GY-016, in part by Science and Technology Innovation Team in Shaanxi Province under Grant 2023-CX-TD-23, and in part by State Key Laboratory of Electrical Insulation and Power Equipment under Grant EIPE22205. Recommended for publication by Associate Editor R. Kennel. *(Corresponding author: Zhonggang Yin.)*

Yangyang Cui, Zhonggang Yin, and Yanping Zhang are with the Department of Electrical Engineering, Xi'an University of Technology, Xi'an 710054, China (e-mail: 1211913014@stu.xaut.edu.cn; zhgyin@xaut.edu.cn; zhangyanping@xaut.edu.cn).

Fengtao Gao is with the Department of Electrical Engineering, Tsinghua University, Beijing 100084, China (e-mail: fengtaogao@mail.tsinghua.edu.cn).

Yiqi Liu is with the College of Mechanical and Electrical Engineering, Northeast Forestry University, Harbin 150040, China (e-mail: ee_617@nefu.edu.cn).

Jing Liu is with the Department of Electronic Engineering, Xi'an University of Technology, Xi'an 710048, China (e-mail: jingliu@xaut.edu.cn).

Color versions of one or more figures in this article are available at https://doi.org/10.1109/TPEL.2023.3340699.

Digital Object Identifier 10.1109/TPEL.2023.3340699

bandwidth frequency, making the physical meaning of ADRC controller parameters more intuitive. Although the difficulties in parameter tuning and theoretical analysis of LADRC have been solved, its tracking speed and antidisturbance ability have also been reduced. At present, the problem of insufficient regulation ability of LADRC in certain applications, such as large time delay system.

Many researchers have made improvements to LADRC and applied it to PMSM drive systems for different types of disturbances and combined them with various operating conditions. In [19], an IPMSM speed loop controller based on a quasi-resonant LADRC is proposed, aimed at suppressing speed fluctuations and torque ripple caused by periodic and aperiodic disturbances. In [20], a LADRC considering velocity measurement noise is proposed and applies it to the SPMSM velocity loop controller, which has a good ability to suppress low-frequency disturbance to the system without affecting its dynamic performance. In [21], a SPMSM speed loop controller bottomed on sliding mode LADRC is proposed, and to enhance the dynamic tracking performance of SPMSM drive systems under both external disturbances and internal parameter changes. In [22], a discrete time repetitive control bottomed on LADRC is proposed, which aims to suppress direct-current and alternating-current disturbances in the current loop of the IPMSM drive system. In [23], the LADRC is mainly used to achieve sensorless control of IPMSM, and compared with the conventional sliding mode controller, the effect of phase delay and speed jitter is reduced. Although the dynamic tracking and antidisturbance abilities of the system have been improved by the improved LADRC proposed previously, the coupling problem between tracking and antidisturbance abilities caused by the influence of observer bandwidth on conventional LADRC (C-LADRC) under different operating conditions and various complex disturbance conditions still cannot be solved. At the same time, the problem of system oscillation can be caused by excessive observer bandwidth, however, the total disturbance may not be accurately estimated and compensated due to the small observer bandwidth.

To solve the abovementioned problem, a series connection leading correction LADRC (SCLC-LADRC) is proposed in this article. As the core of SCLC-LADRC, the SCLC linear extended state observer (SCLC-LESO) is composed of the total disturbance transfer function of the conventional LESO (C-LESO) and a series connection leading correction network. As a result, the estimation range of the LESO for total disturbance is expanded, and the problem of system oscillation caused by excessive observer bandwidth is also solved.

The rest of this article is organized as follows. In Section II, the IPMSM mathematical model is established and the SCLC-LADRC is proposed. Meanwhile, an IPMSM speed loop controller based on C-LADRC and SCLC-LADRC is designed. In Section III, the control performance of SCLC-LADRC is analyzed and the parameter tuning method is provided. In Section IV, the validity and availability of the proposed method are proved through experiments. Finally, Section V concludes this article.

II. Design of IPMSM Speed Loop Controller Based on C-LADRC and Proposal of SCLC-LADRC

A. Design of IPMSM Speed Loop Controller Based on C-LADRC

Coordinate transformation is the foundation of vector control in IPMSM drive systems, and the speed loop controller is mainly influenced by the motion equation. The motion equation of IPMSM is described as follows [24]:

$$\dot{\omega}_r = \frac{1}{\bar{J}}T_e - \frac{1}{\bar{J}}T_L - \frac{\Delta J}{\bar{J}}\dot{\omega}_r - \frac{B_r}{\bar{J}}\omega_r + \delta \tag{1}$$

where ω_r is the mechanical angular velocity, B_r is the damping coefficient, T_e and T_L are the electromagnetic torque and load torque, respectively, δ is the external disturbances, and ΔJ, $\bar{J}$, and J are the changes in rotational inertia, nominal value, and actual value, respectively, and $J = \bar{J}+\Delta J$.

Due to the fact that the motion equation of IPMSM is a first-order differential equation, the first-order LADRC is used as the speed loop controller for the IPMSM drive system [25]. Considering that the research on the method of arranging the transition process in the industrial control field is relatively mature at present, and to avoid the high-frequency oscillation of the system, the linear TD is not used in this article [26]. Therefore, the first-order C-LADRC consists of three major components: 1) second-order LESO, 2) linear state error feedback (LSEF), and 3) total disturbance compensation. For first-order system $\dot{y} = f(y,w,t)+b_0u$, the system output $y = x_1$ and the total disturbance $f = x_2$ are selected as the state variables [27]. The control algorithm is described as follows:

$$\begin{cases} \dot{\hat{x}}_1 = \hat{x}_2 - \beta_1(\hat{x}_1 - x_1) + b_0u \\ \dot{\hat{x}}_2 = -\beta_2(\hat{x}_1 - x_1) \\ u_0 = k_p(r - \hat{x}_1) \\ u = u_0 - \frac{\hat{x}_2}{b_0} \end{cases} \tag{2}$$

where $\hat{x}_1$ and $\hat{x}_2$ are the estimated values of state variables x_1 and x_2, respectively, β_1 and β_2 is the LESO feedback gain coefficient, b_0 is the compensation factor (also known as control gain), k_p is the controller proportional gain coefficient, r is the given input value, and u_0 is the output of LSEF.

By pole assignment, the observer feedback gain coefficient is configured at the observer bandwidth ω_o, the proportional gain coefficient of the controller is configured at the controller bandwidth ω_c [28]

$$\begin{cases} s^2 + \beta_1 s + \beta_2 = (s + \omega_o)^2 \\ s + k_p = s + \omega_c. \end{cases} \tag{3}$$

From (3), it can be concluded that $\beta_1 = 2\omega_o$, $\beta_2 = \omega 2\ o$, $k_p = \omega_c$.

According to (1), the output ω_r of the system is selected as the state variable, and its state equation is described as follows:

$$\dot{\omega}_r = f + b_0T_e \tag{4}$$

where

$$\begin{cases} b_0 = \frac{1}{\bar{J}} \\ f = -\frac{\Delta J}{\bar{J}}\dot{\omega}_r - \frac{1}{\bar{J}}T_L - \frac{B_r}{\bar{J}}\omega_r + \delta \end{cases}. \tag{5}$$

As shown in (5), b_0 is configured as the nominal value $1/\bar{J}$ of the moment of inertia. The error ΔJ generated by the actual and nominal values of the moment of inertia is included as an internal disturbance within the total disturbance.

In (5), both external and internal disturbances suffered by the system are included in the total disturbance $x_2 = f$. Where external disturbance refers to the disturbance imposed by the external system (such as given disturbance and load disturbance). Internal disturbances refer to internal changes in the system (such as structural changes, temperature drift, zero drift, and changes in system parameters).

From the abovementioned analysis, it can be concluded that the IPMSM speed loop control algorithm based on C-LADRC is described as follows:

$$\begin{cases} \dot{\hat{\omega}}_r = \hat{f} - 2\omega_o\left(\hat{\omega}_r - \omega_r\right) + b_0 T_e \\ \dot{\hat{f}} = -\omega_o^2\left(\hat{\omega}_r - \omega_r\right) \\ u_0 = \omega_c\left(\omega_r^* - \hat{\omega}_r\right) \\ T_e = u_0 - \frac{\hat{f}}{b_0} \end{cases} \tag{6}$$

where $\hat{\omega}_r$ and $\hat{f}$ are estimated values of ω_r and f, respectively. ω_r^* is the reference value for the given mechanical angular velocity.

B. Series Connection Leading Correction Linear Active Disturbance Rejection Controller

According to (2) and (3), the Laplace transform of C-LESO is described as follows:

$$\begin{cases} \hat{X}_1(s) = \frac{2\omega_o s + \omega_o^2}{s^2 + 2\omega_o s + \omega_o^2} Y(s) + \frac{b_0 s}{s^2 + 2\omega_o s + \omega_o^2} U(s) \\ \hat{X}_2(s) = \frac{\omega_o^2 s}{s^2 + 2\omega_o s + \omega_o^2} Y(s) - \frac{b_0 \omega_o^2}{s^2 + 2\omega_o s + \omega_o^2} U(s) \end{cases} \tag{7}$$

where $\hat{X}_1(s)$, $\hat{X}_2(s)$, $Y(s)$, and $U(s)$ are Laplace transforms of $,x_1$, x_2, y, and u, respectively.

For the first-order system state equation $\dot{y} = f + b_0 u$, the Laplace transformation formula is described as follows:

$$sY(s) = F(s) + b_0 U(s) \tag{8}$$

where $F(s)$ is the Laplace transform of f.

The transfer function of C-LESO based on the total disturbance f can be obtained by combining (7) and (8) are described as follows:

$$\Phi_C(s) = \frac{\hat{X}_2(s)}{F(s)} = \frac{\omega_o^2}{s^2 + 2\omega_o s + \omega_o^2}. \tag{9}$$

According to (9), $\Phi_C(s)$ is only related to ω_o, and as ω_o increases, the ability to estimate the total disturbance increases. However, the problem of system oscillation can be caused by excessive ω_o [29], [30]. Therefore, in order to broaden the estimation range of LESO for total disturbance, the problem of system oscillation caused by excessive ω_o can be effectively solved, combined with the method of series connection leading correction, $\Phi_C(s)$ is improved as follows:

$$\begin{aligned} \Phi_{\text{SCLC}}(s) &= \frac{\hat{X}_2(s)}{F(s)} \cdot \frac{\alpha T_\alpha s + 1}{T_\alpha s + 1} \\ &= \frac{\omega_o^2}{s^2 + 2\omega_o s + \omega_o^2} \cdot \frac{\alpha T_\alpha s + 1}{T_\alpha s + 1} \end{aligned} \tag{10}$$

where T_α is the lead correction time constant. α is the coefficient, and $\alpha > 1$.

Through the abovementioned analysis, x_3 is introduced as the corrected total disturbance state variable. Let the estimated value of x_3 be $\hat{x}_3$.

The transfer function of the total disturbance based on the SCLC-LESO can be obtained as follows:

$$\begin{aligned} \Phi_{\text{SCLC}}(s) &= \frac{\hat{X}_3(s)}{F(s)} \\ &= \frac{\omega_o^2}{s^2 + 2\omega_o s + \omega_o^2} \cdot \frac{\alpha T_\alpha s + 1}{T_\alpha s + 1} \end{aligned} \tag{11}$$

where $\hat{X}_3(s)$ is the Laplace transform of x_3.

According to (11), the SCLC-LADRC control algorithm is described as follows:

$$\begin{cases} \dot{\hat{x}}_1 = \hat{x}_2 - 2\omega_o\left(\hat{x}_1 - x_1\right) + b_0 u \\ \dot{\hat{x}}_2 = -\omega_o^2\left(\hat{x}_1 - x_1\right) \\ \dot{\hat{x}}_3 = -\alpha\omega_o^2\left(\hat{x}_1 - x_1\right) + \frac{1}{T_\alpha}\left(\hat{x}_2 - \hat{x}_3\right) \\ u_0 = \omega_c\left(r - \hat{x}_1\right) \\ u = u_0 - \frac{\hat{x}_3}{b_0}. \end{cases} \tag{12}$$

From the abovementioned analysis, it can be concluded that the IPMSM speed loop control algorithm based on SCLC-LADRC is described as follows:

$$\begin{cases} \dot{\hat{\omega}}_r = \hat{f} - 2\omega_o\left(\hat{\omega}_r - \omega_r\right) + b_0 T_e \\ \dot{\hat{f}} = -\omega_o^2\left(\hat{\omega}_r - \omega_r\right) \\ \dot{\hat{f}}_\omega = -\alpha\omega_o^2\left(\hat{\omega}_r - \omega_r\right) + \frac{1}{T_\alpha}\left(\hat{f} - \hat{f}_\omega\right) \\ u_0 = \omega_c\left(\omega_r^* - \hat{\omega}_r\right) \\ T_e = u_0 - \frac{\hat{f}_\omega}{b_0} \end{cases} \tag{13}$$

where f_ω is the total disturbance state variable after correction, $\hat{f}_\omega$ is the estimated value of f_ω, and b_0 is still configured as $1/\bar{J}$. According to (5), f is the total disturbance composed of external disturbances (load sudden changes) and internal disturbances (inverter nonlinearity, parameter mismatch, and mechanical friction).

The control structure diagram of IPMSM driver system based on SCLC-LADRC is shown in Fig. 1.

III. Analysis of SCLC-LADRC Control Performance

The primary problem of control system is stability, while the essential problem is antidisturbance. Therefore, the estimation error of SCLC-LESO and antidisturbance characteristic of SCLC-LADRC under different types of disturbances are first analyzed in this section, and parameter tuning methods are provided. Then, the stability of the IPMSM driving system based on SCLC-LADRC is analyzed.

A. Estimation Error Analysis of SCLC-LESO

According to (6), (9), (11), and (13), the estimation error transfer functions of C-LESO and SCLC-LESO based on total disturbance are described as follows:

$$E_C(s) = F(s) - \hat{F}(s) = \frac{s^2 + 2\omega_o s}{s^2 + 2\omega_o s + \omega_o^2} F(s) \tag{14}$$

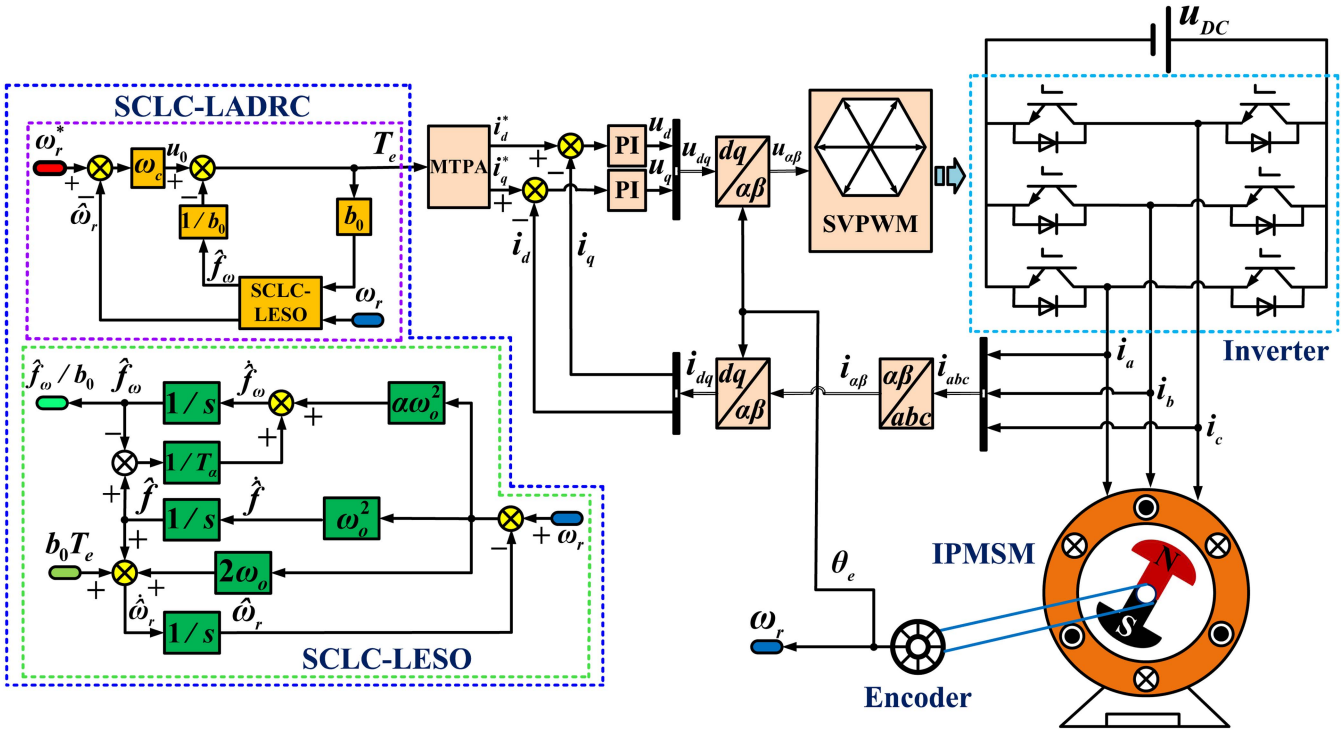

Fig. 1. Control structure diagram of IPMSM driver system based on SCLC-LADRC.

TABLE I
ESTIMATION ERROR OF C-LESO AND SCLC-LESO BASED ON TOTAL DISTURBANCE UNDER DIFFERENT DISTURBANCES

$F(s)$	$\frac{K}{s}$	$\frac{K}{s^2}$		$\frac{K}{s^3}$	
		$(\alpha-1)\omega_o T_\alpha = 2$	$(\alpha-1)\omega_o T_\alpha \neq 2$	$(\alpha-1)\omega_o T_\alpha = 2$	$(\alpha-1)\omega_o T_\alpha \neq 2$
$\lim_{t\to\infty} e_C(t)$	0	$\frac{2K}{\omega_o}$	$\frac{2K}{\omega_o}$	∞	∞
$\lim_{t\to\infty} e_{SCLC}(t)$	0	0	$\frac{K\left[2-(\alpha-1)\omega_o T_\alpha\right]}{\omega_o}$	$\frac{K\left(1+2\omega_o T_\alpha\right)}{\omega_o^2}$	∞

$$E_{\mathrm{SCLC}}(s) = F(s) - \hat{F}_\omega(s) = \frac{(T_\alpha s+1)\left(s^2+2\omega_o s+\omega_o^2\right)-\omega_o^2(\alpha T_\alpha s+1)}{(T_\alpha s+1)(s^2+2\omega_o s+\omega_o^2)}F(s). \tag{15}$$

When $F(s)$ are step perturbation, slope perturbation, and acceleration perturbation, the time-domain expressions for the steady-state errors of C-LESO and SCLC-LESO can be obtained, as shown in (16)–(18) shown at the bottom of next page, respectively. The estimation error of C-LESO and SCLC-LESO based on total disturbance can be obtained from (16)–(18), as shown in Table I.

From Table I, it can be concluded that when $F(s)$ is a step disturbance, the steady-state error of both C-LESO and SCLC-LESO is zero. When the total disturbance is slope disturbance and acceleration disturbance, the steady-state error of both control methods is determined by whether expression $(\alpha\text{-}1)\omega_o T_\alpha$ is equal to 2. For slope disturbances, if $(\alpha\text{-}1)\omega_o T_\alpha = 2$, the system controlled by C-LESO has steady-state error, while the system controlled by SCLC-LESO has zero steady-state error. For acceleration disturbances, although there is a nonzero steady-state error in the SCLC-LESO control system, compared to the infinity steady-state error of C-LESO, the steady-state error of SCLC-LESO can be reduced by increasing ω_o. It can be concluded that compared to C-LESO, the steady-state error caused by slope disturbance can be eliminated by reasonably configuring the values of α, T_α, and ω_o. At the same time, the steady-state error generated by acceleration disturbances can also be reduced.

From the abovementioned analysis, it can be concluded that the following tuning method can be adopted for the time constant

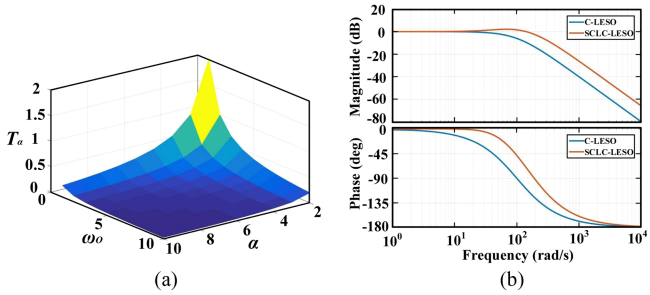

(a) (b)

Fig. 2. Parameter relationship surface of the series connection leading correction network and the Bode Plots of LESO based on total disturbance. (a) Relationship surface between α, T_α, and ω_o. (b) Bode Plots of C-LESO and SCLC-LESO are based on total disturbance.

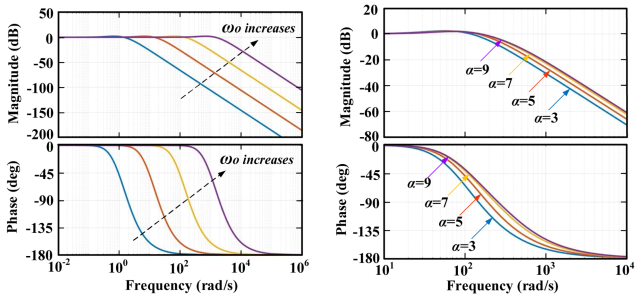

(a) (b)

Fig. 3. Bode Plots of SCLC-LESO based on total disturbance. (a) When ω_o is changed. (b) When α is changed.

T_α of the series connection leading correction network:

$$T_\alpha = \frac{2}{(\alpha-1)\,\omega_o}. \tag{19}$$

The relationship surface between α, T_α, and ω_o is shown in Fig. 2(a).

B. Analysis of Antidisturbance Characteristic

The expression obtained by substituting (19) into (11) is described as follows:

$$\begin{aligned}\Phi_{\text{SCLC}}(s) &= \frac{\hat{X}_3(s)}{F(s)} \\ &= \frac{2\alpha\omega_o^2 s + (\alpha-1)\,\omega_o^3}{2s^3 + (\alpha\omega_o + 3\omega_o)\,s^2 + 2\alpha\omega_o^2 s + (\alpha-1)\,\omega_o^3}.\end{aligned} \tag{20}$$

According to (9) and (20), under the same ω_o conditions, the Bode Plots of C-LESO and SCLC-LESO based on total disturbance are shown in Fig. 2(b). From the figure, it can be concluded that under the same ω_o conditions, compared to C-LESO, the total disturbance estimation range is expanded by SCLC-LESO, and its antidisturbance ability is improved without increasing ω_o. At the same time, the impact of phase lag generated by C-LESO estimation of total disturbance can also be improved by SCLC-LESO.

According to (20), the transfer function of SCLC-LESO based on total disturbance is related to α and ω_o, simultaneously. Therefore, the Bode Plots of SCLC-LESO based on total disturbance can be obtained when α and ω_o are changed separately, as shown in Fig. 3(a) and (b). It can be concluded that the disturbance compensation ability of the system is enhanced with the increase of ω_o, and the impact of phase lag is also improved. But when α is increased to a certain value, its antidisturbance ability is no longer increased. Combining Figs. 2(a) and 3(b), $\alpha = 7$ can be selected as the optimal coefficient for the series leading correction network.

The antidisturbance characteristics of SCLC-LADRC can be further analyzed based on the abovementioned conclusions. The Laplace transform of (13) is described as follows:

$$\begin{cases}\hat{\Omega}_r(s) = \frac{2\omega_o s+\omega_o^2}{s^2+2\omega_o s+\omega_o^2}\Omega_r(s) + \frac{b_0 s}{s^2+2\omega_o s+\omega_o^2}T_e(s) \\ \hat{F}(s) = \frac{\omega_o^2 s}{s^2+2\omega_o s+\omega_o^2}\Omega_r(s) - \frac{b_0\omega_o^2}{s^2+2\omega_o s+\omega_o^2}T_e(s) \\ \hat{F}_\omega(s) = \frac{\alpha T_\alpha\omega_o^2 s^2+\omega_o^2 s}{(T_\alpha s+1)(s^2+2\omega_o s+\omega_o^2)}\Omega_r(s) \\ \qquad - \frac{\alpha T_\alpha\omega_o^2 b_0 s+b_0\omega_o^2}{(T_\alpha s+1)(s^2+2\omega_o s+\omega_o^2)}T_e(s) \\ T_e(s) = \omega_c\Omega_r^*(s) - \omega_c\hat{\Omega}_r(s) - \frac{1}{b_0}\hat{F}_\omega(s)\end{cases} \tag{21}$$

where $\hat{\Omega}_r(s)$, $\Omega_r(s)$, $\Omega_r^*(s)$, $T_e(s)$, and $\hat{F}_\omega(s)$ are the Laplace transforms of $\hat{\omega}_r$, ω_r, ω_r^*, T_e, and $\hat{f}_\omega$, respectively.

$$\begin{cases}e_C(t) = Ke^{-\omega_o t} + K\omega_o t e^{-\omega_o t} \\ e_{\text{SCLC}}(t) = \frac{\left(K+\alpha KT_\alpha^2\omega_o^2-2KT_\alpha\omega_o\right)}{(T_\alpha\omega_o-1)^2}e^{-\omega_o t} - \frac{\left(K\omega_o-\alpha KT_\alpha\omega_o^2\right)}{T_\alpha\omega_o-1}te^{-\omega_o t} + \frac{\left(KT_\alpha\omega_o^2-K\alpha T_\alpha\omega_o^2\right)}{(T_\alpha\omega_o-1)^2}T_\alpha e^{-\frac{1}{T_\alpha}t}\end{cases} \tag{16}$$

$$\begin{cases}e_C(t) = \frac{2K}{\omega_o} - \frac{2K}{\omega_o}e^{-\omega_o t} - Kte^{-\omega_o t} \\ e_{\text{SCLC}}(t) = \frac{2K+KT_\alpha\omega_o-\alpha KT_\alpha\omega_o}{\omega_o} - \frac{2K-3KT_\alpha\omega_o+2K\alpha T_\alpha^2\omega_o^2-K\alpha T_\alpha\omega_o}{\omega_o(T_\alpha\omega_o-1)^2}e^{-\omega_o t} + \frac{K-K\alpha T_\alpha\omega_o}{T_\alpha\omega_o-1}te^{-\omega_o t} \\ \qquad - \frac{\left(KT_\alpha\omega_o^2-K\alpha T_\alpha\omega_o^2\right)}{(T_\alpha\omega_o-1)^2}T_\alpha^2 e^{-\frac{1}{T_\alpha}t}\end{cases} \tag{17}$$

$$\begin{cases}e_C(t) = -\frac{3K}{\omega_o^2} + \frac{2K}{\omega_o}t + \frac{3K}{\omega_o^2}e^{-\omega_o t} + \frac{K}{\omega_o}te^{-\omega_o t} \\ e_{\text{SCLC}}(t) = -\frac{3K+KT_\alpha^2\omega_o^2+2KT_\alpha\omega_o-K\alpha T_\alpha^2\omega_o^2-2K\alpha T_\alpha\omega_o}{\omega_o^2} + \frac{2K+KT_\alpha\omega_o-K\alpha T_\alpha\omega_o}{\omega_o}t \\ \qquad + \frac{3K-4KT_\alpha\omega_o+3K\alpha T_\alpha^2\omega_o^2-2K\alpha T_\alpha\omega_o}{\omega_o^2(T_\alpha\omega_o-1)^2}e^{-\omega_o t} - \frac{K-K\alpha T_\alpha\omega_o}{\omega_o(T_\alpha\omega_o-1)}te^{-\omega_o t} + \frac{T_\alpha^3\left(KT_\alpha\omega_o^2-K\alpha T_\alpha\omega_o^2\right)}{(T_\alpha\omega_o-1)^2}e^{-\frac{1}{T_\alpha}t}.\end{cases} \tag{18}$$

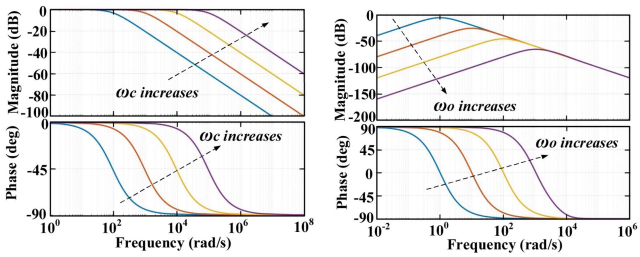

Fig. 4. Bode Plots of SCLC-LADRC tracking and antidisturbance capabilities. (a) Tracking capability. (b) Antidisturbance capability.

According to (4), its Laplace transform is described as follows:

$$T_e(s) = \frac{s}{b_0}\Omega_r(s) - \frac{1}{b_0}F(s). \tag{22}$$

The closed-loop transfer function of SCLC-LADRC based on input and disturbance terms can be obtained by combining (21) and (22) as follows:

$$\Omega_r(s) = \frac{b_0\omega_c}{s+b_0\omega_c}\Omega_r^*(s) + \frac{e_0s^3+e_1s^2+e_2s}{a_0s^4+a_1s^3+a_2s^2+a_3s+a_4}F_\omega(s) \tag{23}$$

where

$$\begin{cases}\beta = \frac{1}{\alpha-1}\\ \gamma = \frac{1}{\omega_o}\end{cases} \tag{24}$$

$$\begin{cases}e_0 = 2\beta\gamma\\ e_1 = 4\beta + 2b_0\beta\gamma\omega_c + 1\\ e_2 = b_0\omega_c\end{cases} \tag{25}$$

$$\begin{cases}a_0 = 2\beta\gamma\\ a_1 = 4\beta + 2b_0\beta\gamma\omega_c + 1\\ a_2 = 2\beta\omega_o + 2\omega_o + 4b_0\beta\omega_c + b_0\omega_c\\ a_3 = \omega_o^2 + 2b_0\beta\omega_c\omega_o + 2b_0\omega_c\omega_o\\ a_4 = b_0\omega_c\omega_o^2.\end{cases} \tag{26}$$

According to (23), the Bode Plots of SCLC-LADRC tracking and disturbance compensation abilities are shown in Fig. 4(a) and (b). From Fig. 4(a), as ω_c increases, its tracking characteristic is enhanced. From Fig. 4(b), by increasing ω_o, the disturbance gain of the system can be reduced, the disturbance compensation capability of the system can be also enhanced.

As shown in Figs. 3(a) and 4, the antidisturbance ability of the system increases with the increase of ω_o. But excessive ω_o can lead to system oscillation. Therefore, the digital control system is limited by the discrete time delay characteristic, the ω_o must be less than $2/T_s$ (where T_s is the sampling time). And there is a relationship of $\omega_o = (3\text{–}5)\omega_c$ between ω_o and ω_c [31].

Therefore, when the range of values for ω_o and ω_c is determined, first, the ω_o should be selected from the minimum initial value, and then ω_o should gradually increase until the system requirements are difficult to meet by the influence of noise. Next, the ω_o is gradually reduced until the optimal parameter value that meets the dynamic requirements of the system is adjusted. Throughout the entire adjustment process, $\omega_o = (3\text{–}5)\omega_c$ must always be maintained.

C. Analysis of Stability

The stability analysis of IPMSM control system based on SCLC-LADRC should be conducted from two aspects: 1) control gain uncertainty and 2) model parameter uncertainty [32]. First, the uncertainty of control input gain is considered. The inaccurate value of control gain b_0 not only affects the control effect of the entire closed-loop control system, but also affects the stability of the system [33]. Therefore, the first step is to analyze whether adopting the $b_0 = 1/\bar{J}$ configuration method in this article will have an impact on the stability of the system. According to (1), the following expression can be obtained:

$$\dot{\omega}_r = -\frac{1}{J}T_L - \frac{B_r}{J}\omega_r + \delta + (b-b_0)T_e + b_0T_e \tag{27}$$

where

$$\begin{cases}f = -\frac{1}{J}T_L - \frac{B_r}{J}\omega_r + \delta + (b-b_0)T_e\\ b = \frac{1}{J}\\ b_0 = \frac{1}{\bar{J}}.\end{cases} \tag{28}$$

In (27) and (28), only a portion of the information in b is considered known, and the known portion is represented as b_0.

For the convenience of theoretical analysis, the influence of external disturbances and model parameter uncertainty is not considered temporarily. From the abovementioned analysis, it can be concluded that the total disturbance f at this time is described as follows:

$$f = (b-b_0)T_e. \tag{29}$$

The Laplace transform of (29) is described as follows:

$$F(s) = (b-b_0)T_e(s). \tag{30}$$

The closed-loop transfer function of the system can be obtained by simplifying (22)–(26) and (30) is described as follows:

$$\frac{\Omega_r(s)}{\Omega_r^*(s)} = \frac{s_0s^3+s_1s^2+s_2s+s_3}{l_0s^4+l_1s^3+l_2s^2+l_3s+l_4} \tag{31}$$

where

$$\begin{cases}s_0 = 2bb_0\omega_c\beta\gamma\\ s_1 = 4bb_0\omega_c\beta + bb_0\omega_c\\ s_2 = 2bb_0\omega_c\omega_o\beta + 2bb_0\omega_c\omega_o\\ s_3 = bb_0\omega_c\omega_o^2\end{cases} \tag{32}$$

$$\begin{cases}l_0 = 2b_0\beta\gamma\\ l_1 = 4b_0\beta + 2b_0^2\omega_c\beta\gamma + b_0\\ l_2 = 4bb_0\omega_c\beta + 2b\omega_o\alpha\beta + b_0^2\omega_c\\ l_3 = b\omega_o^2 + 2bb_0\omega_c\omega_o\beta + 2bb_0\omega_c\omega_o\\ l_4 = bb_0\omega_c\omega_o^2.\end{cases} \tag{33}$$

Since l_0, l_1, l_2, l_3, l_4 are all greater than zero, the odd-order Hurwitz [34] determinant is described as follows:

$$\begin{cases} \Delta_1 = a_1 > 0 \\ \Delta_3 = \begin{vmatrix} l_1 & l_3 & 0 \\ l_0 & l_2 & l_4 \\ 0 & l_1 & l_3 \end{vmatrix} = l_1\left(l_2 l_3 - l_1 l_4\right) - l_0 l_3^2 > 0 \end{cases}. \tag{34}$$

From (34), it can be concluded that the odd-order Hurwitz determinant is greater than zero. Therefore, according to the Liénard-Chipard stability criterion [35], the compensation factor b_0 is configured as $1/\bar{J}$, which can ensure that the IPMSM control system based on SCLC-LADRC is a stable system.

Second, the uncertainty of model parameters is considered.

The controlled object is described as follows:

$$\Omega_r(s) = \frac{b_0}{s + k_c} T_e(s) \tag{35}$$

where k_c is an unknown parameter.

The closed-loop transfer function of the system can be obtained by combining (22)–(26) and (35) as follows:

$$\frac{\Omega_r(\mathrm{s})}{\Omega_r^*(s)} = \frac{m_0 s^3 + m_1 s^2 + m_2 s + m_3}{n_0 s^4 + n_1 s^3 + n_2 s^2 + n_3 s + n_4} \tag{36}$$

where

$$\begin{cases} m_0 = 2b_0\omega_c\beta\gamma \\ m_1 = 4b_0\omega_c\beta + b_0\omega_c \\ m_2 = 2b_0\omega_c\omega_o\beta + 2b_0\omega_c\omega_o \\ m_3 = b_0\omega_c\omega_o^2 \end{cases} \tag{37}$$

$$\begin{cases} n_0 = 2\beta\gamma \\ n_1 = 2\beta\gamma k_c + 4\beta + 2b_0\omega_c\beta\gamma + 1 \\ n_2 = (4\beta + 2b_0\omega_c\beta\gamma + 1)k_c + 2\omega_o\beta + 2\omega_o + 4b_0\omega_c\beta + b_0\omega_c \\ n_3 = b_0\omega_c k_c + \omega_o^2 + 2b_0\omega_c\omega_o\beta + 2b_0\omega_c\omega_o \\ n_4 = b_0\omega_c\omega_o^2. \end{cases} \tag{38}$$

From (36)–(38), when $k_c \geq 0$, the stability of the system can be obtained from Hurwitz Stability Criterion.

When $k_c < 0$, first, it is necessary to find that all coefficients of the system characteristic equation are greater than zero, k_c needs to be satisfied by the set relationship represented of the following equation Q:

$$Q = M \cap N \cap P \tag{39}$$

where

$$\begin{cases} M = \left\{ k_c \middle| k_c > -\frac{4\beta + 2b_0\omega_c\beta\gamma + 1}{2\beta\gamma} \right\} \\ N = \left\{ k_c \middle| k_c > -\frac{2\omega_o\beta + 2\omega_o + 4b_0\omega_c\beta + b_0\omega_c}{4\beta + 2b_0\omega_c\beta\gamma + 1} \right\} \\ P = \left\{ k_c \middle| k_c > -\frac{\omega_o^2 + 2b_0\omega_c\omega_o\beta + 2b_0\omega_c\omega_o}{b_0\omega_c} \right\}. \end{cases} \tag{40}$$

Second, it is necessary to satisfy that the odd-order Hurwitz determinant is greater than zero, which is described as follows:

$$\begin{cases} \Delta_1 = n_1 > 0 \\ \Delta_3 = \begin{vmatrix} n_1 & n_3 & 0 \\ n_0 & n_2 & n_4 \\ 0 & n_1 & n_3 \end{vmatrix} = n_1 n_2 n_3 - n_1^2 n_4 - n_0 n_3^2 > 0 \end{cases}. \tag{41}$$

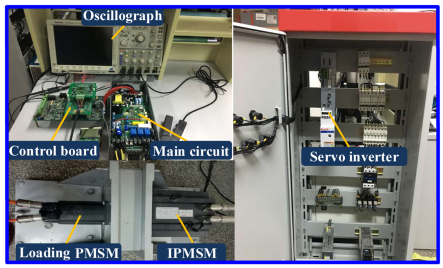

Fig. 5. IPMSM vector control experimental platform.

For the first-order Hurwitz determinant, the following conclusion can be obtained from (38) and (41):

$$k_c > -\frac{4\beta + 2b_0\omega_c\beta\gamma + 1}{2\beta\gamma}. \tag{42}$$

For the third-order Hurwitz determinant, the stability of the system cannot be directly determined due to the unknown parameter k_c in its expansion.

Therefore, it can be simplified as a cubic equation $f(k_c)$ with unknown parameter k_c, which is described as follows:

$$\begin{aligned} f(k_c) = {} & c_0 c_1 c_2 k_c^3 + (c_0 c_2 d_2 + c_1 c_2 d_1 \\ & + c_0 c_1 d_3 - c_0^2 d_4 - c_2^2 d_0) k_c^2 \\ & + (c_2 d_1 d_2 + c_0 d_2 d_3 + c_1 d_1 d_3 \\ & - 2c_0 d_1 d_4 - 2c_2 d_0 d_3) k_c \\ & + d_1 d_2 d_3 - d_1^2 d_4 - d_0 d_3^2 \end{aligned} \tag{43}$$

where

$$\begin{cases} c_0 = 2\beta\gamma \\ c_1 = 4\beta + 2b_0\omega_c\beta\gamma + 1 \\ c_2 = b_0\omega_c \end{cases} \tag{44}$$

$$\begin{cases} d_0 = 2\beta\gamma \\ d_1 = 4\beta + 2b_0\omega_c\beta\gamma + 1 \\ d_2 = 2\omega_o\beta + 2\omega_o + 4b_0\omega_c\beta + b_0\omega_c \\ d_3 = \omega_o^2 + 2b_0\omega_c\omega_o\beta + 2b_0\omega_c\omega_o \\ d_4 = b_0\omega_c\omega_o^2. \end{cases} \tag{45}$$

Assuming that k_{c1}, k_{c2}, and k_{c3} are the three roots of $f(k_c) = 0$, and $k_{c1} < k_{c2} < k_{c3}$. Therefore, when $k_{c1} < k_c < k_{c2}$ or $k_c > k_{c3}$, the system is stable.

Based on the abovementioned analysis, the IPMSM control system based on SCLC-LADRC is stable in engineering sense. And its tracking ability and antidisturbance ability are better than C-LADRC.

IV. Experimental Verification

To verify the correctness and effectiveness of the control method proposed in this article, the 2-kW IPMSM vector control experimental platform is built, as shown in Fig. 5. Where the TMS320F28335 chip is selected as the system core processor. The motor parameters are shown in Table II.

To achieve a fair and effective comparison between C-LADRC and SCLC-LADRC controllers, the ω_o and ω_c of the

TABLE II
MOTOR PARAMETERS

Parameter	Parameter Value
Rated power (kW)	2
Rated voltage (V)	380
Rated current (A)	5.8
Rated frequency (Hz)	66.67
Rated speed (rpm)	1000
Polar logarithm	4
d-axis inductance (H)	0.01085
q-axis inductance (H)	0.02552
Moment of inertia (kg·m^2)	0.011
Stator resistance (Ω)	1.351
Permanent magnet flux linkage (Wb)	0.77

TABLE III
CONTROLLER PARAMETERS

Parameter	Parameter value
α	7
b_0	90.91
ω_o (rad/s)	100
ω_c (rad/s)	25

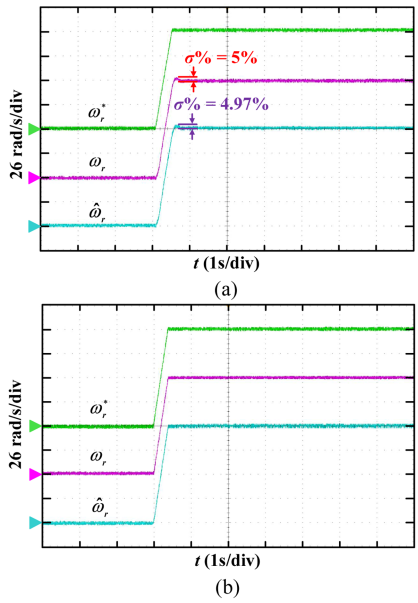

Fig. 6. Speed waveform of IPMSM during rated no-load operation. (a) C-LADRC. (b) SCLC-LADRC.

two controllers are configured with the same parameter values according to the parameter tuning principles in Section III-B, as shown in Table III.

A. Verification of Tracking Characteristic

The given angular velocity ω_r^*, actual angular velocity ω_r, and estimated angular velocity $\hat{\omega}_r$ waveforms of IPMSM under rated no-load operating conditions controlled by two different controllers are shown in Fig. 6.

From Fig. 6, it can be concluded that when controlled by C-LADRC, the IPMSM has a 5% overshoot at the moment of startup, and there is a tracking error of 0.03% between the actual speed and the estimated speed. When controlled by SCLC-LADRC, the IPMSM does not overshoot at the moment of startup and can be achieved with an error free estimation of the given speed. This indicates that SCLC-LADRC has better tracking characteristic than C-LADRC, and also indicates that SCLC-LESO has better estimation ability than C-LESO.

B. Verification of Antidisturbance Characteristic

To effectively verify the antidisturbance characteristic of the control method proposed in this article in combination with different operating conditions, the antidisturbance characteristic between the two controllers under rated-speed and extremely low-speed operating conditions will be compared and analyzed in this section. The characteristic of the motor speed during extremely low-speed operation is the presence of significant speed fluctuations. The reasons for this include frictional torque, harmonic torque (including ripple torque and cogging torque), uneven internal structure of the motor, inverter nonlinearity, and unstable power supply voltage. Where the main reason for the low-speed fluctuation phenomenon of the motor is caused by friction torque. Because when the motor operates at extremely low-speed, the influence of the motor will be further exacerbated by nonlinear frictional resistance, resulting in stable changes in the input at low-speed, while the output of the system is a pulsating change. The accuracy and stability of motors operating at extremely low-speed can be affected by speed fluctuations, which may lead to equipment failures in severe cases. Therefore, the suppression of extremely low-speed oscillation is first compared and analyzed by different controllers in this section.

The steady-state waveforms of the no-load given angular velocity, actual angular velocity, estimated angular velocity, and total disturbance of IPMSM at 1 Hz no-load operating frequency are shown in Fig. 7. The actual angular velocity and U-phase current waveform of IPMSM during loading and unloading at 1 Hz operating frequency are shown in Fig. 8.

From Fig. 7, it can be concluded that under extremely low-speed no-load operation conditions, when controlled by C-LADRC, the actual speed offset of IPMSM is ±0.1 rad/s, and there is an estimation error of ±0.015 rad/s between the actual speed and the estimated speed. When controlled by SCLC-LADRC, the actual speed offset is ±0.05 rad/s, and there is an estimation error of ±0.003 rad/s between the actual speed and the estimated speed. This indicates that SCLC-LADRC has better ability to suppress speed fluctuations at extremely low-speed compared to C-LADRC, and also indicates that SCLC-LESO has better steady-state estimation ability for speed and total disturbance at extremely low-speed compared to C-LESO.

From Fig. 8, it can be concluded that under extremely low-speed operating conditions, when controlled by C-LADRC, the actual speed drop during loading is 13.3%, and the adjustment time is 0.2 s. The actual speed overshoot during unloading is also 13.3%, and the adjustment time is 0.19 s. When controlled by SCLC-LADRC, the actual speed drop during loading is 8%,

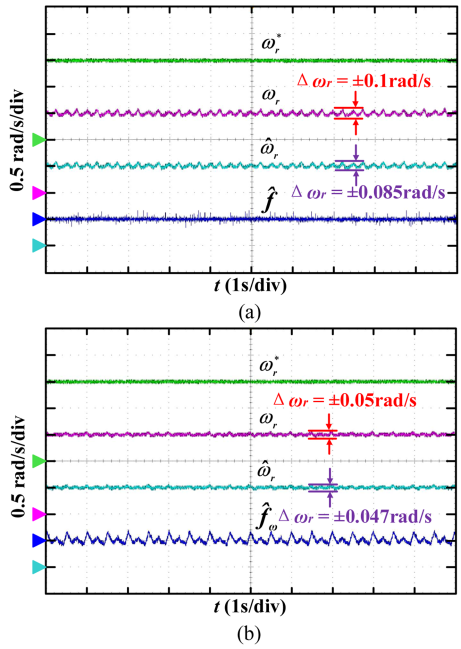

Fig. 7. Speed and total disturbance waveforms of IPMSM during extremely low-speed no-load operating conditions. (a) C-LADRC. (b) SCLC-LADRC.

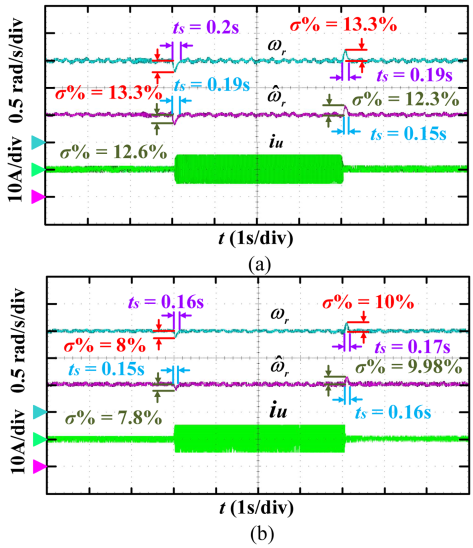

Fig. 8. Speed and current waveform of IPMSM during loading and unloading under extremely low-speed operating conditions. (a) C-LADRC. (b) SCLC-LADRC.

and the adjustment time is 0.16 s. The actual speed overshoot during unloading is 10%, and the adjustment time is 0.17 s. This indicates that SCLC-LADRC has better antidisturbance ability than C-LADRC under extremely low-speed operating conditions.

At the same time, the estimation errors of speed overshoot, speed drop, and adjustment time under extremely low-speed operating conditions are shown in Tables IV and V, respectively. From the table, it can be concluded that when controlled by C-LADRC, the estimated error of the speed drop during loading is 0.7%, and the estimated error of the adjustment time is 0.01 s. The estimation error of the speed overshoot during unloading is 1%, and the estimation error of the adjustment time is 0.04 s. When controlled by SCLS-LADRC, the estimation error of the speed drop during loading is 0.2%, and the estimation error of the adjustment time is also 0.01 s. The estimation error of the speed overshoot during unloading is 0.02%, and the estimation error of the adjustment time is 0.01 s. Thus, it can be proven that SCLC-LESO has better dynamic estimation performance compared to C-LESO.

TABLE IV
ESTIMATION ERROR OF SPEED OVERSHOOT AND SPEED DROP UNDER EXTREMELY LOW-SPEED OPERATING CONDITIONS

$\Delta\sigma$%	Drop	Overshoot
C-LADRC	0.7%	1%
SCLC-LADRC	0.2%	0.02%

TABLE V
ESTIMATION ERROR OF ADJUSTMENT TIME UNDER EXTREMELY LOW-SPEED OPERATING CONDITIONS

Δt_s	Drop	Overshoot
C-LADRC	0.01 s	0.04 s
SCLC-LADRC	0.01 s	0.01 s

The reason for the speed fluctuation of the motor during extremely low-speed operation indicates that this fluctuation is periodic, but the frequency is relatively low, so it can be considered as a low-frequency disturbance. From Fig. 2(b), it can be concluded that SCLC-LESO is equivalent to a low-pass filter, and under the same ω_o conditions, compared to C-LESO, the estimated range of total disturbance is widened by SCLC-LESO, and the problem of system oscillation caused by excessive ω_o is solved. Therefore, by adjusting ω_o reasonably, the low-frequency disturbance that cause speed fluctuation under extremely low-speed operating conditions can be effectively estimated, and the total disturbance including low-frequency disturbance that cause speed fluctuation can be effectively compensated through feedforward compensation. For C-LADRC, speed fluctuation under extremely low-speed operating conditions can also be suppressed by further increasing ω_o. However, under the same ω_o conditions, compared to C-LADRC, the speed fluctuation of the motor under extremely low-speed operating conditions can be effectively suppressed by SCLC-LADRC. Moreover, if ω_o in C-LADRC continues to increase, the whole system oscillation is highly likely to oscillate, leading to system instability.

The actual angular velocity, estimated angular velocity, torque, and *U*-phase current waveforms of IPMSM during loading and unloading under rated-speed operating conditions controlled by two different controllers are shown in Fig. 9.

From the figure, it can be concluded that under rated-speed operating conditions, when controlled by C-LADRC, the actual speed drop during loading is 8.9%, and the adjustment time is 0.2 s. The actual speed overshoot during unloading is 8.4%, and the adjustment time is 0.21 s. However, when controlled by SCLC-LADRC, the actual speed drop during loading is 4.9%, and the adjustment time is 0.1 s. The actual speed overshoot

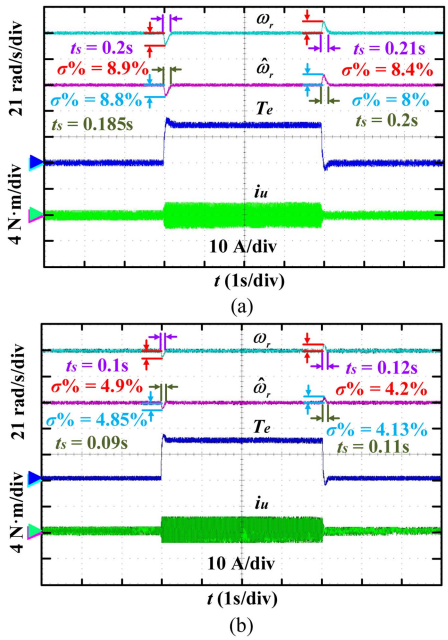

Fig. 9. Speed, torque, and current waveforms of IPMSM when loaded and unloaded during rated-speed operating conditions. (a) C-LADRC. (b) SCLC-LADRC.

TABLE VI
ESTIMATION ERROR OF SPEED OVERSHOOT AND SPEED DROP UNDER RATED-SPEED OPERATING CONDITIONS

Δσ%	J		2J		0.5J	
	Drop	Overshoot	Drop	Overshoot	Drop	Overshoot
C-LADRC	0.1%	0.4%	2%	0.3%	1.2%	1%
SCLC-LADRC	0.05%	0.07%	0.5%	0.3%	0.9%	0.05%

TABLE VII
ESTIMATION ERROR OF ADJUSTMENT TIME UNDER RATED-SPEED OPERATING CONDITIONS

Δt_s	J		2J		0.5J	
	Drop	Overshoot	Drop	Overshoot	Drop	Overshoot
C-LADRC	0.015 s	0.01 s	0.04 s	0.02 s	0.03 s	0.01 s
SCLC-LADRC	0.01 s	0.01 s	0.005 s	0.007 s	0.01 s	0.006 s

during unloading is 4.2%, and the adjustment time is only 0.12 s. This further demonstrates that SCLC-LADRC has better tracking and antidisturbance abilities than C-LADRC.

At the same time, the estimation errors of speed overshoot, speed drop, and adjustment time under rated-speed operating conditions are shown in Tables VI and VII, respectively. From the table, it can be concluded that when controlled by C-LADRC, the estimated error of the speed drop during loading is 0.1%, and the estimated error of the adjustment time is 0.015 s. The estimation error of the speed overshoot during unloading is 0.4%, and the estimation error of the adjustment time is 0.01 s. When controlled by SCLS-LADRC, the estimation error of the speed drop during loading is 0.05%, and the estimation error of the adjustment time is also 0.01 s. The estimation error of the speed overshoot during unloading is 0.07%, and the estimation error of the adjustment time is 0.01 s. Thus, it can be further proven

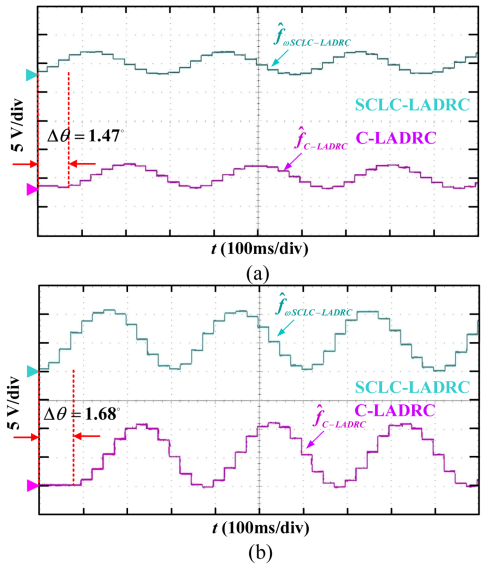

Fig. 10. Total disturbance waveform during loading under different speed operating conditions. (a) Rated-speed. (b) Extremely low-speed.

that SCLC-LESO has better dynamic estimation performance compared to C-LESO.

The total disturbance waveform estimated by SCLC-LESO and C-LESO under different speed loading operating conditions is shown in Fig. 10. From the figure, it can be concluded that under the rated-speed loading operating conditions, the total disturbance estimated by C-LESO lags by 1.47° compared to the total disturbance estimated by SCLC-LESO. Under extremely low-speed loading operating conditions, the total disturbance estimated by C-LESO lags by 1.68° compared to the total disturbance estimated by SCLC-LESO. It can be verified that compared to C-LESO, the problem of insufficient tracking ability and antidisturbance ability caused by total disturbance phase lag in the system can be improved by SCLC-LESO.

C. Verification of Robustness

The control performance of IPMSM is not only affected by different types of external disturbances, but also by internal uncertainties such as changes in system parameters. To verify the robustness of the control method proposed in this article to parameter changes, a series of comparative experiments are conducted under inertia mismatch and rated-speed operating conditions in this section.

The actual angular velocity, estimated angular velocity, torque, and current waveforms of IPMSM controlled by two different controllers with increasing and decreasing moment of inertia are shown in Figs. 11 and 12, respectively. The data comparison of speed drop, speed overshoot, and adjustment time under inertia mismatch conditions is shown in Figs. 13 and 14, respectively. The estimation errors of speed overshoot, speed drop, and adjustment time under inertia mismatch rated-speed operating conditions are shown in Tables VI and VII, respectively.

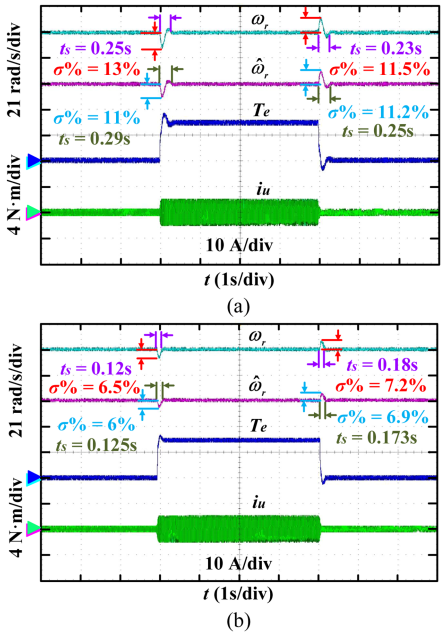

Fig. 11. Speed, torque, and current waveforms of IPMSM during loading and unloading under inertial mismatch and rated-speed operating conditions (J increased to $2J$). (a) C-LADRC. (b) SCLC-LADRC.

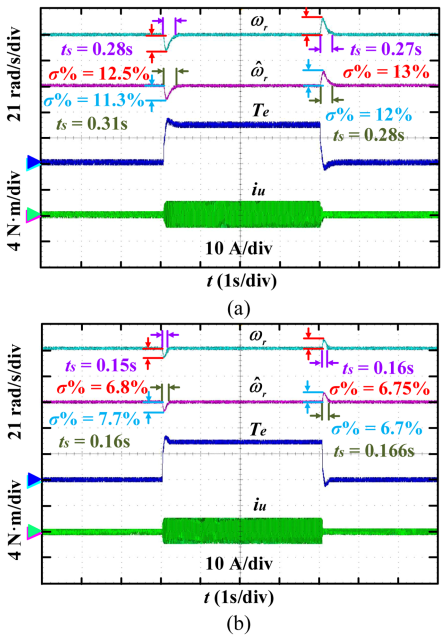

Fig. 12. Speed, torque, and current waveforms of IPMSM during loading and unloading under inertial mismatch and rated-speed operating conditions (J decreased to $0.5J$). (a) C-LADRC. (b) SCLC-LADRC.

From Figs. 11–14, it can be concluded that when J is not mismatched, compared to C-LADRC, the speed drop of SCLC-LADRC at the moment of loading is reduced by 4%, and the adjustment time is shortened by 0.1 s. At the moment of unloading, the speed overshoot is reduced by 4.2%, and the adjustment time is shortened by 0.09 s. When J is increased to $2J$, compared to C-LADRC, the speed drop of SCLC-LADRC at

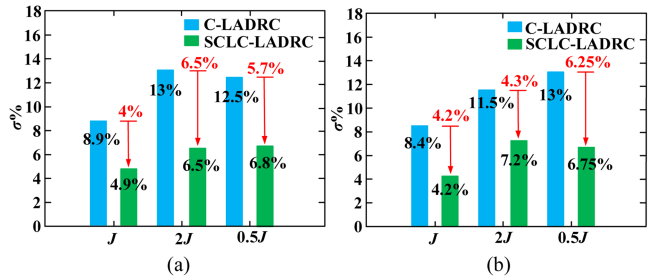

Fig. 13. Comparison of speed drop and speed overshoot indicators during IPMSM loading and unloading under inertial mismatch and rated-speed operating conditions. (a) Load. (b) Unload.

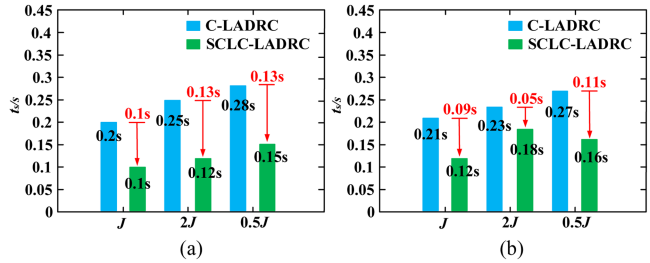

Fig. 14. Comparison of adjustment time indicators for IPMSM loading and unloading under inertial mismatch and rated-speed operating conditions. (a) Load. (b) Unload.

the moment of loading is reduced by 6.5%, and the adjustment time is shortened by 0.13 s. At the moment of unloading, the speed overshoot is reduced by 4.3%, and the adjustment time is shortened by 0.05 s. Similarly, when J is reduced to $0.5J$, compared to C-LADRC, the speed drop of SCLC-LADRC at the moment of loading is reduced by 5.7%, and the adjustment time is shortened by 0.13 s. At the moment of unloading, the speed overshoot is reduced by 6.25%, and the adjustment time is shortened by 0.11 s. From the abovemenntioned analysis, it can be concluded that under the condition of inertia mismatch, the SCLC-LADRC has stronger parameter robustness compared to C-LADRC.

At the same time, from Tables VI and VII, it can be concluded that when J is increased to $2J$ and the system is controlled by C-LADRC, the estimated error of speed drop during loading is 2%, and the estimated error of adjustment time is 0.04 s. The estimation error of the speed overshoot during unloading is 0.3%, and the estimation error of the adjustment time is 0.02 s. When controlled by SCLS-LADRC, the estimated error of speed drop during loading is 0.5%, and the estimated error of adjustment time is 0.005 s. The estimation error of the speed overshoot during unloading is 0.3%, and the estimation error of the adjustment time is 0.007s. Meanwhile, when J is reduced to $0.5J$ and the system is controlled by C-LADRC, the estimated error of the speed drop during loading is 1.2%, and the estimated error of the adjustment time is 0.03 s. The estimation error of the speed overshoot during unloading is 1%, and the estimation error of the adjustment time is 0.01 s. When controlled by SCLS-LADRC, the estimated error of the speed drop during loading is 0.9%, and the estimated error of the adjustment time

is also 0.01 s. The estimation error of the speed overshoot during unloading is 0.05%, and the estimation error of the adjustment time is 0.006 s.

V. Conclusion

To solve the coupling problem of tracking and antidisturbance of C-LADRC under different operating and disturbance conditions due to the influence of bandwidth, a SCLC-LADRC is proposed in this article. Based on the IPMSM motion equation, a speed loop controller based on SCLC-LADRC is designed. Meanwhile, the estimation performance of SCLC-LESO, the antidisturbance performance of SCLC-LADRC, and the stability of the system are analyzed. Finally, the validity and availability of the proposed method are proved through experiments. Theoretical analysis and experimental results indicates that the introduction of a series leading correction network not only broadens the estimation range of LESO for total disturbance, avoids system oscillation problem caused by excessive ω_o, but also improves the estimation accuracy of LESO for total disturbance. Therefore, compared to C-LADRC, the SCLC-LADRC has been proven to have better tracking capability, antidisturbance capability, robustness, and certain engineering application value.

References

[1] G. Wang, R. Liu, N. Zhao, D. Ding, and D. Xu, "Enhanced linear ADRC strategy for HF pulse voltage signal injection-based sensorless IPMSM drives," *IEEE Trans. Power Electron.*, vol. 34, no. 1, pp. 514–525, Jan. 2019.

[2] S. Bhattacharjee, S. Halder, Y. Yan, A. Balamurali, L. V. Lyer, and N. C. Kar, "Real-time SIL validation of a novel PMSM control based on deep deterministic policy gradient scheme for electrified vehicles," *IEEE Trans. Power Electron.*, vol. 37, no. 8, pp. 9000–9011, Aug. 2022.

[3] M. Lee and K. Nam, "Subdomain approach for IPMSM via an equivalent SPMSM model," in *Proc. 21st Int. Conf. Elect. Mach. Syst.*, 2018, pp. 2719–2724.

[4] Y. Zhang, Z. Yin, C. Bai, G. Wang, and J. Liu, "A rotor position and speed estimation method using an improved linear extended state observer for IPMSM sensorless drives," *IEEE Trans. Power Electron.*, vol. 36, no. 12, pp. 14062–14073, Dec. 2021.

[5] M. Tian, B. Wang, Y. Yu, Q. Dong, and D. Xu, "Static-errorless deadbeat predictive current control for PMSM current harmonics suppression based on vector resonant controller," *IEEE Trans. Power Electron.*, vol. 38, no. 4, pp. 4585–4595, Apr. 2023.

[6] S. Chen, W. Ding, R. Hu, X. Wu, and S. Shi, "Sensorless control of PMSM drives using reduced order quasi resonant-based ESO and Newton-Raphson method-based PLL," *IEEE Trans. Power Electron.*, vol. 38, no. 1, pp. 229–244, Jan. 2023.

[7] P. Chen and Y. Luo, "Analytical fractional-order PID controller design with Bode's ideal cutoff filter for PMSM speed servo system," *IEEE Trans. Ind. Electron.*, vol. 70, no. 2, pp. 1783–1793, Feb. 2023.

[8] X. Zhang, B. Wang, Y. Yu, J. Zhang, and D. Xu, "Torque adaptive hexagon voltage extension method for PMSM flux-weakening control based on dual PI cascade structure," *IEEE Trans. Power Electron.*, vol. 38, no. 1, pp. 332–345, Jan. 2023.

[9] M. Zhang and X. Jing, "Model-free saturated PD-SMC method for 4-DOF tower crane systems," *IEEE Trans. Ind. Electron.*, vol. 69, no. 10, pp. 10270–10280, Oct. 2022.

[10] X. Li, M. Xiao, M. Ji, J. Yang, X. Wu, and G. Shen, "Restraint of common-mode voltage for PMSM-inverter systems with current ripple constraint based on voltage-vector MPC," *IEEE J. Emerg. Sel. Topics Ind. Electron.*, vol. 4, no. 2, pp. 688–697, Apr. 2023.

[11] C. Bai, Z. Yin, J. Luo, P. Luo, and J. Liu, "Robust composite finite-time convergent speed control of induction machine based on multiple sources disturbance estimation technology generalized proportional integral observer," *IEEE J. Emerg. Sel. Topics Power Electron.*, vol. 10, no. 5, pp. 6160–6170, Oct. 2022.

[12] R. Zhang, Z. Yin, N. Du, J. Liu, and X. Tong, "Robust adaptive current control of a 1.2-MW direct-drive PMSM for traction drives based on internal model control with disturbance observer," *IEEE Trans. Transp. Electrific.*, vol. 7, no. 3, pp. 1466–1481, Sep. 2021.

[13] Z. Wang, A. Yu, X. Li, G. Zhang, and C. Xia, "A novel current predictive control based on fuzzy algorithm for PMSM," *IEEE J. Emerg. Sel. Topics Power Electron.*, vol. 7, no. 2, pp. 990–1001, Jun. 2019.

[14] J. Hang, X. Shu, S. Ding, and Y. Huang, "Robust open-circuit fault diagnosis for PMSM drives using wavelet convolutional neural network with small samples of normalized current vector trajectory graph," *IEEE Trans. Ind. Electron.*, vol. 70, no. 8, pp. 7653–7663, Aug. 2023.

[15] W. Lu et al., "Load adaptive PMSM drive system based on an improved ADRC for manipulator joint," *IEEE Access*, vol. 9, pp. 33369–33384, 2021.

[16] J. Han, "From PID to active disturbance rejection control," *IEEE Trans. Ind. Electron.*, vol. 56, no. 3, pp. 900–906, Mar. 2009.

[17] S. Chen, Z. Chen, and Z.-L. Zhao, "Parameter selection and performance analysis of linear disturbance observer based control for a class of nonlinear uncertain systems," *IEEE Trans. Ind. Electron.*, vol. 70, no. 11, pp. 11587–11597, Nov. 2023.

[18] Z. Gao, "Scaling and bandwidth-parameterization based controller tuning," in *Proc. IEEE. Amer. Control Conf.*, 2003, pp. 4989–4996.

[19] B. Wang, M. Tian, Y. Yu, Q. Dong, and D. Xu, "Enhanced ADRC with quasi-resonant control for PMSM speed regulation considering aperiodic and periodic disturbances," *IEEE Trans. Transp. Electrific.*, vol. 8, no. 3, pp. 3568–3577, Sep. 2022.

[20] Y. Zuo, J. Mei, C. Jiang, X. Yuan, S. Xie, and C. H. T. Lee, "Linear active disturbance rejection controllers for PMSM speed regulation system considering the speed filter," *IEEE Trans. Power Electron.*, vol. 36, no. 12, pp. 14579–14592, Dec. 2021.

[21] L. Qu, W. Qiao, and L. Qu, "An extended-state-observer-based sliding-mode speed control for permanent-magnet synchronous motors," *IEEE J. Emerg. Sel. Topics Power Electron.*, vol. 9, no. 2, pp. 1605–1613, Apr. 2021.

[22] M. Tian, B. Wang, Y. Yu, Q. Dong, and D. Xu, "Discrete-time repetitive control-based ADRC for current loop disturbances suppression of PMSM drives," *IEEE Trans. Ind. Inform.*, vol. 18, no. 5, pp. 3138–3149, May 2022.

[23] B. Du, S. Wu, S. Han, and S. Cui, "Application of linear active disturbance rejection controller for sensorless control of internal permanent-magnet synchronous motor," *IEEE Trans. Ind. Electron.*, vol. 63, no. 5, pp. 3019–3027, May 2016.

[24] Z. Yin, Y. Zhang, X. Cao, D. Yuan, and J. Liu, "Estimated position error suppression using novel PLL for IPMSM sensorless drives based on full-order SMO," *IEEE Trans. Power Electron.*, vol. 37, no. 4, pp. 4463–4474, Apr. 2022.

[25] C. Liu, G. Luo, X. Duan, Z. Chen, Z. Zhang, and C. Qiu, "Adaptive LADRC-based disturbance rejection method for electromechanical servo system," *IEEE Trans. Ind. Appl.*, vol. 56, no. 1, pp. 876–889, Jan./Feb. 2020.

[26] Y. Wang, L. Tao, P. Wang, X. Ma, P. Cheng, and D. Zhao, "Improved linear ADRC for hybrid energy storage microgrid output-side converter," *IEEE Trans. Ind. Electron.*, vol. 69, no. 9, pp. 9111–9120, Sep. 2022.

[27] W. Xue, R. Madonski, K. Lakomy, Z. Gao, and Y. Huang, "Add-on module of active disturbance rejection for set-point tracking of motion control systems," *IEEE Trans. Ind. Appl.*, vol. 53, no. 4, pp. 4028–4040, Jul./Aug. 2017.

[28] L. Tao, P. Wang, X. Ma, Y. Wang, and H. Shi, "Robustness optimization through modified linear active disturbance rejection control for high-voltage load interface in microgrid," *IEEE Trans. Ind. Electron.*, vol. 70, no. 4, pp. 3909–3919, Apr. 2023.

[29] C. Wang, J. Yan, P. Heng, L. Shan, and X. Zhou, "Enhanced LADRC for permanent magnet synchronous motor with compensation function observer," *IEEE J. Emerg. Sel. Topics Power Electron.*, vol. 11, no. 3, pp. 3424–3434, Jun. 2023.

[30] F. Yang et al., "Complex coefficient active disturbance rejection controller for current harmonics suppression of IPMSM drives," *IEEE Trans. Power Electron.*, vol. 37, no. 9, pp. 10443–10454, Sep. 2022.

[31] B. Zhang, W. Tan, and J. Li, "Tuning of linear active disturbance rejection control via frequency domain approximation," *Control Theory Appl.*, vol. 36, no. 5, pp. 831–840, 2018.

[32] H. Jin and K. Huang, "Root locus and b_0 selection of first-order linear active disturbance rejection control systems," in *Proc. IEEE 10th Data Driven Control Learn. Syst. Conf.*, 2021, pp. 917–921.

[33] Y. Huang, W. Xue, and X. Yang, "Active disturbance rejection control: Methodology, theoretical analysis and applications," in *Proc. 29th Chin. Control Conf.*, 2010, pp. 6083–6090.

[34] D. Ke, F. Wang, L. He, and Z. Li, "Predictive current control for PMSM systems using extended sliding mode observer with Hurwitz-based power reaching law," *IEEE Trans. Power Electron.*, vol. 36, no. 6, pp. 7223–7232, Jun. 2021.
[35] E. I. Jury, "A simplified stability criterion for linear discrete systems," *Proc. Int. Rev. Educ.*, vol. 50, no. 6, pp. 1493–1500, Jun. 1962.

Yangyang Cui was born in Shandong, China, in 1996. He received the B.S. degree in electrical engineering and automation from the Binzhou University, Binzhou, China, in 2018 and the M.S. degree in electrical engineering from the Tianjin University of Technology, Tianjin, China, in 2021. He is currently working toward the Ph.D. degree in electrical engineering with Xi'an University of Technology, Xi'an, China.

His current research interest includes active disturbance rejection control of permanent magnet synchronous motor.

Zhonggang Yin (Member, IEEE) was born in Shandong, China, in 1982. He received the B.S., M.S., and Ph.D. degrees in electrical engineering from Xi'an University of Technology, Xi'an, China, in 2003, 2006, and 2009, respectively.

In 2009, he was with the Department of the Electrical Engineering, Xi'an University of Technology, where he is currently a Professor. His research interests include high-performance control of ac motor and digital control of power converters.

Fengtao Gao was born in Shaanxi Province, China, in 1994. He received the B.S., M.S., and Ph.D. degrees in electrical engineering from Xi'an University of Technology, Xi'an, China, in 2016, 2019, and 2023, respectively.

He is currently a Postdoctoral Research Fellow with the Department of Electrical Engineering, Tsinghua University, Beijing, China. His research interests include synchronous reluctance machine drives and condition monitoring, and diagnostics for electric machine drives.

Yanping Zhang (Member, IEEE) was born in Shannxi, China, in 1989. He received the B.S. degree from Xi'an Polytechnic University, Shaanxi, China, in 2013, and the M.S. and Ph.D. degrees from Xi'an University of Technology, Shaanxi, China, in 2017 and 2021, respectively, all in electrical engineering.

In 2021, he was with the Department of Electrical Engineering, Xi'an University of Technology, where he is currently a Lecturer. His research interest includes high performance sensorless control of synchronous motor.

Yiqi Liu (Member, IEEE) received the B.S. degree from Northeast Agriculture University, Harbin, China, in 2009, the M.S. degree from the Tianjin University of Technology, Tianjin, China, in 2012, and the Ph.D. degree from the Harbin Institute of Technology, Harbin, China, in 2016, all in electrical engineering.

From 2013 to 2015, he was a Visiting Ph.D. Student with the Center for Ultra-Wide-Area Resilient Electric Energy Transmission Networks, University of Tennessee, Knoxville, TN, USA, with support from the China Scholarship Council. In 2016, he has been an Associate Professor with Northeast Forestry University, Harbin, China. His current research interests include power electronics for renewable energy sources, multilevel converters, high-voltage direct-current technology, dc microgrids and energy conversion, and wireless power transfer systems.

Jing Liu was born in Anhui, China, in 1982. She received the B.S., M.S., and Ph.D. degrees in electronic engineering from Xi'an University of Technology, Xi'an, China, in 2003, 2006, and 2009, respectively.

In 2009, she has been an Associate Professor with the Department of Electronic Engineering, Xi'an University of Technology. Her research interests include the power semiconductor devices and their application to power electronic devices.